OPEN

Journal of Cerebral Blood Flow & Metabolism (2015) 35, 1711–1721

www.jcbfm.com

ORIGINAL ARTICLE

Multimodal imaging reveals temporal and spatial microglia and matrix metalloproteinase activity after experimental stroke

Bastian Zinnhardt[1], Thomas Viel[1,2], Lydia Wachsmuth[3], Alexis Vrachimis[1,4], Stefan Wagner[4], Hans-Jörg Breyholz[4], Andreas Faust[1,4,5], Sven Hermann[1,4,5], Klaus Kopka[4,5,11], Cornelius Faber[3,5], Frédéric Dollé[6], Sabina Pappata[7], Anna M Planas[8], Bertrand Tavitian[2], Michael Schäfers[1,4,5], Lydia M Sorokin[5,9], Michael T Kuhlmann[1] and Andreas H Jacobs[1,5,10]

Stroke is the most common cause of death and disability from neurologic disease in humans. Activation of microglia and matrix metalloproteinases (MMPs) is involved in positively and negatively affecting stroke outcome. Novel, noninvasive, multimodal imaging methods visualizing microglial and MMP alterations were employed. The spatio-temporal dynamics of these parameters were studied in relation to blood flow changes. Micro positron emission tomography (μPET) using [^{18}F]BR-351 showed MMP activity within the first days after transient middle cerebral artery occlusion (tMCAo), followed by increased [^{18}F]DPA-714 uptake as a marker for microglia activation with a maximum at 14 days after tMCAo. The inflammatory response was spatially located in the infarct core and in adjacent (penumbral) tissue. For the first time, multimodal imaging based on PET, single photon emission computed tomography, and magnetic resonance imaging revealed insight into the spatio-temporal distribution of critical parameters of poststroke inflammation. This allows further evaluation of novel treatment paradigms targeting the postischemic inflammation.

Journal of Cerebral Blood Flow & Metabolism (2015) **35,** 1711–1721; doi:10.1038/jcbfm.2015.149; published online 1 July 2015

Keywords: microglia; matrix metalloproteases; perfusion; positron emission tomography; stroke

INTRODUCTION

Cerebral ischemia is followed by a variety of cellular and molecular alterations. In the cascade of molecular changes after acute cerebral ischemia inflammatory cells and proteases, such as matrix metalloproteinases (MMPs), are known to be key factors in contributing to tissue damage and also to tissue repair functions.

An important group of inflammatory cells activated as a response to ischemia are microglial cells, a subset of glial cells that constantly survey the central nervous system for pathogens and damage. Depending on the activation state, microglial cells fulfill various roles in stroke pathogenesis. Either they exhibit a detrimental function by releasing pro-inflammatory cytokines and chemotactic proteins, thereby amplifying the inflammatory reaction, or they have a beneficial function by promoting repair processes.[1] Upon activation, microglial cells express the 18-kDa mitochondrial translocator protein (TSPO) that has been identified as a characteristic marker for microglial activation.[2,3]

Microglia express a number of proteases, including the latent forms (zymogens) of MMP-2 and MMP-9, which are well characterized as key factors involved in brain damage.[4] The MMP activation has been reported to cause blood–brain barrier damage that is associated with hemorrhagic transformation after acute ischemic stroke.[5] Matrix metalloproteinases are considered to be components of the acute inflammatory reaction after stroke.[6,7] Most importantly, MMPs are capable of modulating inflammatory and immune responses by processing signaling molecules and by affecting cell migration.[8] In agreement with these observations, early inhibition of MMP-9 activity in experimental stroke has beneficial effects on stroke outcome.[9] In contrast to acute MMP inhibition, it was also shown that late inhibition can have detrimental effects, leading to increased brain damage characterized by reductions in neurons and newly formed blood vessels.[10]

Advanced *in vivo* imaging approaches evaluating the temporal and spatial dynamics of inflammatory alterations after stroke might improve our understanding of the different activation states of microglia and MMPs and impact on tissue outcome. This is of particular importance for the evaluation of therapeutic attempts

[1]European Institute for Molecular Imaging (EIMI), Westfälische Wilhelms University Münster, Münster, Germany; [2]Paris Centre de Recherche Cardiovasculaire (PARC), Paris, France; [3]Department of Clinical Radiology of the University Hospital, Westfälische Wilhelms University Münster, Münster, Germany; [4]Department of Nuclear Medicine of the University Hospital, Westfälische Wilhelms University Münster, Münster, Germany; [5]Cells-in-Motion Cluster of Excellence (EXC 1003—CiM), Westfälische Wilhelms University Münster, Münster, Germany; [6]Service Hospitalier Frédéric Joliot, Institut d'Imagerie BioMédicale, CEA, Orsay, France; [7]Institute of Biostructure and Bioimaging, CNR, Naples, Italy; [8]Institut d'Investigacions Biomèdiques de Barcelona, Consejo Superior de Investigaciones Científicas (CSIC), Institut d'Investigacions Biomèdiques August Pi i Sunyer (IDIBAPS), Barcelona, Spain; [9]Institute of Physiological Chemistry and Pathobiochemistry, Westfälische Wilhelms University Münster, Münster, Germany and [10]Department of Geriatrics, Johanniter Hospital, Evangelische Kliniken, Bonn, Germany. Correspondence: Professor AH Jacobs, European Institute for Molecular Imaging (EIMI), University of Münster, Waldeyerstrasse 15, Münster 48149, Germany.
E-mail: ahjacobs@uni-muenster.de
[11]Current address: Radiopharmaceutical Chemistry, German Cancer Research Center (dkfz), Heidelberg, Germany.
This research was partly funded by a fellowship of the 'Cells-in-Motion Cluster of Excellence (EXC 1003—CiM) Graduate School, and the International Max-Planck Research School-Molecular Biomedicine (IMPRS-MBM) Joint Graduate Program' to BZ, and the EU 7th Framework Programme (FP7/2007-2013) under grant agreement n° 278850 (INMiND), and by the Interdisciplinary Center for Clinical Research (IZKF core unit PIX), Münster, Germany.
Received 10 December 2014; revised 11 May 2015; accepted 15 May 2015; published online 1 July 2015

aimed at modulating postischemic inflammation and tissue remodeling to improve clinical outcome of patients.[1]

Approaches employing *in vivo* micro positron emission tomography (μPET) for imaging of microglial activation focus on radiolabelled compounds binding to TSPO. The newly developed probe *N,N*-diethyl-2-(2-(4-(2-[^{18}F]fluoroethoxy)phenyl)-5,7-dimethylpyrazolo[1,5-*a*]pyrimidin-3-yl)acetamide ([^{18}F]DPA-714) binds with high affinity to TSPO and has been evaluated in rat models of cerebral ischemia, experimental autoimmune encephalomyelitis, and cancer (reviewed by Jacobs *et al*[1]). For PET imaging of MMPs, the (*R*)-2-(*N*-benzyl-4-(2-[^{18}F]fluoroethoxy)phenylsulphonamido)-*N*-hydroxy-3-methylbutanamide compound CGS 27023A 1 ([^{18}F]BR-351), a radiofluorinated MMP inhibitor, has been developed.[11] [^{18}F]BR-351 is a selective nonpeptidyl broad spectrum inhibitor of MMPs characterized by favorable IC_{50} values for activated MMP-2 and -9. Due to its underlying molecular structure, [^{18}F]BR-351 can effectively bind to the activated forms of MMP-2, -8, -9, and -13, while the latent forms are not recognized.

The aims of the current study are (1) to evaluate the temporal and spatial evolution of microglia and MMP activation after focal cerebral ischemia in a mouse model of transient middle cerebral artery occlusion (tMCAo) employing [^{18}F]DPA-714 and [^{18}F]BR-351 μPET, respectively; (2) to validate temporal and spatial interactions of microglia and MMP activity by immunohistochemistry; and (3) to correlate μPET findings to perfusion deficits evaluated by [^{99m}Tc]-hexamethylpropyleneamine oxime ([^{99m}Tc]HMPAO) and micro single photon emission computed tomography (μSPECT) as well as to structural stroke outcome as measured by T2-weighted (T2w) micro magnetic resonance imaging (μMRI).

MATERIALS AND METHODS

Study Design

Multimodality imaging based on μPET and μMRI was applied to investigate the spatial and temporal dynamics of microglial and MMP activation in a murine model of transient stroke in relation to cerebral blood flow measurements and histologic markers.

Experiments were in accordance with the German Law on the Care and Use of Laboratory Animals and approved by the Landesamt für Natur, Umwelt und Verbraucherschutz of North Rhine-Westphalia and ARRIVE guidelines. C57BL/6 mice were housed at constant temperature (23°C) and relative humidity (40%) under a regular light/dark schedule. Food and water were available *ad libitum*. Samples sizes were determined by power analysis during the animal ethics dossier application.

A total of $N = 31$ of 63 mice underwent μPET and μMRI-T2w imaging studies, respectively. An additional set of $n = 14$ mice were subjected to μSPECT imaging to assess the severity of focal cerebral ischemia at day 1 after tMCAo and its correlation with microglia and/or MMP activity as well as tissue outcome 14 days after tMCAo. Eighteen animals died during the experimental procedures. Fourteen mice underwent [^{99m}Tc]HMPAO μSPECT at 24 hours and μMRI-T2w at 14 days, whereas $n = 6$ of 14 mice were assessed at days 14 and 15 by μPET using [^{18}F]DPA-714 and [^{18}F] BR-351, respectively. In the main group of $n = 31$ animals, mice were subjected to dual μPET imaging with [^{18}F]DPA-714 and [^{18}F]BR-351 for assessment of microglia (TSPO) and MMP activity at different stages after tMCAo (24 to 48 hours ($n = 8$), 7 ± 1 days ($n = 8$), 14 ± 1 days ($n = 8$), 21 ± 1 days ($n = 7$)). T2w-μMRI was performed at the same time of μPET studies in all animals. In addition, $n = 4$ sham operated animals, 7 days after tCMAo, were included in the study. The experimental setup is summarized in Supplementary Figure 1. According to this protocol, multimodal [^{18}F] DPA-714 μPET, [^{18}F]BR-351 μPET, and T2w-μMRI data were available in the same animal for each time point. After each imaging time point, mice were killed. All mice with successful multimodal imaging were included in the data analysis and fixed for immunohistochemistry. No outliers were excluded from the study.

Transient Middle Cerebral Artery Occlusion Surgery

In all, $N = 63$, 3 to 4 months old, male C57BL/6 mice (22 to 25 g body weight) underwent right tMCAo (30 minutes), using an intraluminal occlusion model as described elsewhere with minor modifications.[12] In short, mice were anesthetized with 1.5% isoflurane (Abbott Animal Health, Abbott Park, IL, USA) in 100% O_2. After preparing the right external common carotid artery, a 7-0 monofilament (tip diameter 190 to 200 μm, coating length 2 to 3 mm, 70SPRePK5, Doccol Corp., Sharon, MA, USA), was inserted in the external common carotid artery and positioned at the point where the MCA branches out. Successful occlusion was maintained for 30 minutes before retracting the filament allowing reperfusion. Reduction in blood flow was monitored intraoperatively via a Laser Doppler probe (Periflux 5000, Perimed Instruments, Järfälla, Sweden) attached to the skull of the mouse (Supplementary Figure 2). In the sham operated animals, the filament was shortly inserted into the external common carotid artery and immediately retracted.

Mice were kept under 1.5% isoflurane anesthesia in 100% oxygen throughout the procedure. Body temperature was maintained at physiologic level with a custom built heating pad.

Radiochemistry

[^{18}F]DPA-714 was prepared following the procedure described in the literature with a radioactive purity of 99% and a decay corrected yield (rcy) of $23 \pm 5\%$.[13] The synthesis and quality control of [^{18}F]BR-351 was performed in accordance to Wagner *et al*.[11] Briefly, in a computer controlled TRACERLabFx FN Synthesiser the batch of aqueous [^{18}F]fluoride ions from the cyclotron target was passed through an anion exchange resin (Sep-Pak Light Waters Accell Plus QMA cartridge, ABX GmbH, Radeberg, Germany). [^{18}F]Fluoride ions were eluted from the resin with a mixture of 40 μL 1 mol/L K_2CO_3, 200 μL water for injection, and 600 μL CH_3CN containing 19 mg Kryptofix 2.2.2 (K 222) (ABX GmbH, Radeberg, Germany). Subsequently, the aqueous [^{18}F]K(K 222) solution was carefully evaporated to dryness *in vacuo*. An amount of 3.1 mg (5.4 μmol) of precursor compound (R)-2-(4-(N-Benzyl-N-(1-(hydroxyamino)-3-methyl-1-oxobutan-2-yl)sulphamoyl) phenoxy)ethyl-4-methyl-benzenesulphonate in 1 mL CH_3CN was added, and the mixture was heated at 84 °C for 20 minutes. The mixture was cooled to 50°C, diluted with 9 mL water and passed through a Waters Sep-Pak Light C18 cartridge. The cartridge was washed with additional 5.5 mL water for injection and eluted with 1 mL absolute N,N-dimethylformamide. The undiluted eluate was purified by the radio-RP-HPLC system of the radiosynthesizer. The product fraction of compound [^{18}F]BR-351 was collected and diluted with 50 mL water. The resulting solution was passed through a Waters Sep-Pak Light C18 cartridge. The cartridge was eluted with 1 mL ethanol and the eluate was diluted with 9 mL saline. Finally, the solution of the target compound [^{18}F]BR-351 was dispensed into a sterile pyrogen-free 20 mL glass vial by passing through a 0.22 μm sterile filter. [^{18}F]BR-351 was produced with a radioactive purity of 98% and rcy of 21%.

Anesthesia

Mice were anesthetized with 1.5% isoflurane (Abbott Animal Health) in 100% O_2. The lateral tail vein was cannulated using a 26 Ga catheter (Vasculon Plus, BD, Heidelberg, Germany) connected to a 15-cm polyethylene tubing (27 Ga, Smith Medical, Kent, UK).

Micro Single Photon Emission Computed Tomography Studies

A subgroup of $n = 14$ mice underwent [^{99m}Tc]HMPAO μSPECT imaging at day 1 combined with T2w-μMRI 14 ± 1 days after tMCAo.

Hexamethylpropyleneamine oxime (HMPAO; Stabilised Ceretec, General Electric Company, Fairfield, CT, USA) was supplied in commercially available kits. Each vial was reconstituted with [^{99m}Tc]NaTc-PertechnetateO_4^- according to the manufacturer's instructions. In all, 27.1 ± 5.6 MBq (>96% purity) of [^{99m}Tc]HMPAO was injected. For image acquisition, we used a 4-head gamma camera equipped with multi-pinhole collimators and a cone beam computed tomography (μCT) imaging system (NanoSPECT/CT-Plus preclinical camera; Mediso Medical Imaging Systems, Budapest, Hungary).[14]

Images were acquired 10 minutes after radiotracer injection. Thereafter, a μSPECT acquisition of the skull was initiated, with a scan time of 35 minutes. Further scan parameters were as follows: Energy window level 126 to 154.5 keV, frame duration 150 seconds, number of projections 10, field of view 24 mm, CT voltage 55 kVp. Images were reconstructed by an ordered-subsets expectation maximization algorithm software (HiSPECT; SciVis GMBH, Göttingen, Germany) and the quantitative image analysis was performed using the VivoQuant (inviCRO, Boston, MA, USA) analysis software. To derive radioactivity concentrations in the brain a volume of interest (VOI) was drawn in the visually assessed stroke area on

the SPECT data set. A second VOI placed in cerebellum was used as a reference.

Micro Positron Emission Tomography Studies

At different time points after tMCAo (24 to 48 hours, 7 days, 14 days, and 21 days) and sham surgery (7 days), mice were subjected to μPET imaging using the radiotracers [^{18}F]DPA-714 and [^{18}F]BR-351 for assessment of TSPO expression and MMP activity, respectively.

Micro PET studies were performed on a high-resolution small animal PET scanner (32 module quadHIDAC, Oxford Positron Systems Ltd., Oxford, UK) with uniform spatial resolution (< 1 mm FWHM (full-width at half-maximum)) over a large cylindrical field-of-view (165 mm diameter, 280 mm axial length). The μPET data were reconstructed using one-pass list mode expectation maximization algorithm with resolution recovery.[15] [^{18}F]DPA-714 μPET images were acquired 45 to 75 minutes after intravenous injection of 10 MBq [^{18}F]DPA-714. [^{18}F]BR-351 μPET images were acquired 95 to 110 minutes after intravenous injection of 10 MBq [^{18}F]BR-351.

After each μPET acquisition, the animal bed was transferred into the μCT scanner (Inveon, Siemens Medical Solutions, Knoxville, TN, USA) to acquire μCT images with a spatial resolution of 80 μm. The μCT images were used for anatomic coregistration with the μPET images using a landmark-based approach. In short, three molecular sieve spheres (Acros Organics, Geel, Belgium) (two on the left side and one at the right side of the animal bed) were rinsed in radiotracer solution and taped onto the animal bed. The μPET and μCT images were fused using the landmark tool of the open source image analysis software VINCI (Version: 4.19.0; http://www.nf.mpg.de/vinci3/).[16]

Magnetic Resonance Imaging Studies

The μMRI was performed with a 9.4-T small animal MR scanner with 20 cm bore size (Bios-Spec 94/20; BrukerBioSpin MRI GmbH, Ettlingen, Germany). The system was operated using the software ParaVision 5.1. (BrukerBioSpin MRI GmbH). We used the helium-cooled Cryoprobe (BrukerBioSpin MRI GmbH) to obtain anatomic 2D T2w RARE brain images in three imaging planes (28 planes, slice thickness 0.5 mm, in-plane resolution 78 μm^2 (repetition time 3,000 to 5,500 ms, echo time 50 ms, rare factor 16, 6 averages, 14 to 28 contiguous slices, slice thickness 0.5 mm, field of view 20 mm^2, 256 matrix, in-plane resolution 78 μm^2, scan time 5 to 9 minutes, respectively).

The μMRI was conducted for identification of stroke location, volume, and coregistration to μPET and μSPECT images.

Data Analysis

Image data were analyzed using the VINCI software.[16] The μCT images superimposed to μPET and μSPECT images were coregistered to MRI images using anatomic landmarks and 'Contour-' and 'Fusion-tool' provided by the VINCI software.

The obtained PET/CT images were superimposed to μMRI by using the automatic contour tool, reliably delineating the skull of the mice. The skull contour was further manually superimposed onto the μMRI data using anatomic landmarks. Several structures were used for optimal anatomic coregistration. Example regions were the paraflocculus region (MR) and its respective bone structure (CT); the temporomandibular joint region, the sphenoidal bone, the bulbus olfactorius region, and the lambda region (thickening of the skull dividing the visual cortex from midbrain and cerebellum on top of the inferior colliculus). All coregistrations were verified thoroughly in all 3D image planes.

For the μMRI-based analysis, VOIs were manually drawn into each slice of the coronal MR images. We segmented two different VOIs: (1) the stroke area was identified by the hyperintense signal on T2-weighted images; (2) a comparable second VOI of comparable size and location was drawn in the contralateral hemisphere. These VOIs were copied on μSPECT/μPET images for calculation of regional uptake.

The μPET data were analyzed using μMRI-based analysis, blinded for the μPET imaging results. The μPET tracer uptake was expressed as percentage of injected dose by dividing counts per milliliter in the VOI by total counts obtained in a VOI that included the entire animal, multiplied by 100 (% ID/cc). Lesion-to-contralateral ratios (L/C) were calculated between the ischemic and the contralateral control hemispheres. Hemispheric VOIs were drawn on the obtained PET/CT images of the sham group. Ipsilateral to contralateral uptake ratios (I/C) were calculated.

The μSPECT data were expressed as standardized uptake values, calculated by dividing the tissue radioactivity concentration by the injected activity multiplied by the bodyweight of the mouse.

To investigate interrelations between blood flow disturbance, microglia and MMP activity and stroke size, percentage infarct size relative to whole brain size were calculated for each mouse from the T2w-μMRI data and correlated to the percentage of remaining relative cerebral blood flow (rCBF) in the ipsilateral hemisphere. For correlation with μPET imaging parameters, the percentage of remaining rCBF in the ipsilateral hemisphere 24 hours after tMCAo was correlated to the tracer uptake (%ID) for [^{18}F]DPA-714 and [^{18}F]BR-351, respectively.

Immunohistochemistry

After the last imaging examination, mice were killed and perfused with 4% PFA. Brains were dissected, fixed overnight in 4% PFA, embedded in paraffin and cut in 5 μm coronal sections. Immunohistochemistry was performed for all animals using the paraffin-embedded coronal brain sections employing antibodies for microglia (1:2,000, goat anti Iba-1, ab107159, Abcam, Cambridge, UK), MMP-9 (1:200, rabbit anti-mouse MMP-9, ab38889, Abcam), and TSPO (1:250, rabbit, anti-TSPO, NBP1-95674, Novus Biologicals, Cambridge, UK).

Antigen retrieval was performed by boiling the slides in citrate buffer (pH 6; 30 minutes). Slides were then treated with blocking solution for 30 minutes (1%BSA and 0.5% Triton-X in PBS), subsequently incubated (4°C, overnight) with the primary antibodies for Iba-1 (1:2,000), MMP-9 (1:200), and TSPO (1:250), respectively, followed by incubation with Alexa Fluor 488-conjugated anti-rabbit secondary antibody (1:800, A-21206, Life Technologies, Carlsbad, CA, USA), or Alexa Fluor 555 conjugated anti-goat (1:800, A-21432, Life Technologies, Carlsbad, CA, USA). For conventional histology for TSPO and MMP-9, slides were incubated with a biotinylated goat anti-rabbit (1:800, 45 minutes, B21078, Life Technologies, Darmstadt, Germany), followed by HRP-Streptavidin incubation (20 minutes, K1016, DAKO, Hamburg, Germany). Slides were incubated with 3,3-Diaminobenzidine (D-5637, Sigma, Hamburg, Germany) for 5 minutes. Sections were counterstained with hematoxylin, dehydrated, and mounted using Entellan (Merck, Darmstadt, Germany). The MMP-9 immunofluorescence was taken from the infarct core, whereas the TSPO immunfluorescence was taken from core-to-periinfarct regions.

Slides were mounted in DAPI containing mounting medium (Vectashield, H-1500, Vector Laboratories, Burlingame, CA, USA). Images were acquired with a combined fluorescence-light microscope (Nikon Eclipse NI-E, Nikon, Tokyo, Japan).

Statistical Analysis

All statistical analyses were performed using Sigma Plot 11.0 software package (Systat Software, Erkrath, Germany). Data are expressed as mean ± s.d. All comparisons were tested for normality and variance homogeneity using the Sigma Plot software. Differences between VOIs in ipsilateral and contralateral hemispheres were tested using a paired *t*-test, eventually followed by Mann–Whitney *U*-test on ranks. Overall temporal differences in radiotracer uptake were tested with a one-way analysis of variance (ANOVA) ([^{18}F]BR-351) or a Kruskal–Wallis ANOVA on ranks, followed by pairwise multiple comparison procedures (Dunn's Method/Holm–Sidak method). Correlation analyses were performed using the Spearman correlation analyses. The interhemispheric difference in the sham group was analyzed using paired *t*-tests. Comparisons with the experimental group were performed with an unpaired *t*-test with Welch's correction.

Significance levels were set at $P < 0.05$.

RESULTS

Relative Cerebral Blood Flow Perfusion Deficits Correlate with the Percentage of Infarcted Brain 14 Days After Transient Middle Cerebral Artery Occlusion

[^{99m}Tc]-Hexamethylpropyleneamine oxime μSPECT images revealed mild to severe rCBF reductions 24 hours after tMCAo in the ipsilateral right hemisphere compared with the contralateral left control region. Calculation of [^{99m}Tc]HMPAO uptake ratios between the hemispheres showed an average reduction of the ipsilateral rCBF of 64.3 ± 22.2%. The degrees of perfusion deficits ranged from severe with a remaining ipsilateral rCBF reduced to less than 40% of contralateral values ($n = 4$) (Figure 1A

first row, B), to mild and moderate changes of remaining ipsilateral rCBF (51% to 85%; $n = 10$) (Figure 1A second row, B). T2-weighted μMRI of the same animals at 14 days after tMCAo revealed various infarct sizes, which were correlated to the severity of perfusion deficit observed at 24 hours after tMCAo ($R^2 = 0.66$; $P = 0.003$; $n = 14$) (Figures 1A and 1B).

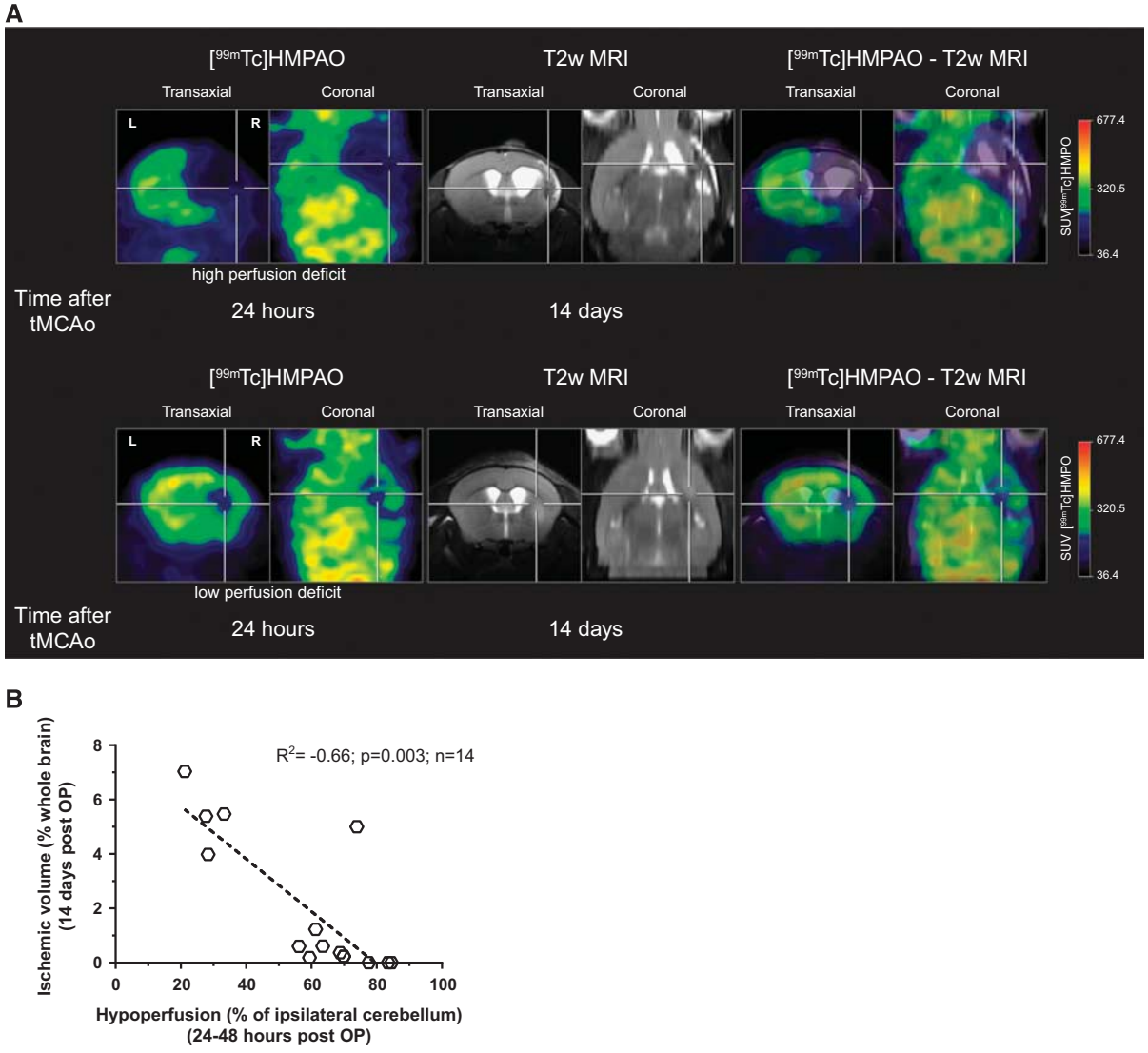

Figure 1. Micro single photon emission computed tomography (μSPECT) of relative cerebral blood flow (rCBF) 24 hours after transient middle cerebral artery occlusion (tMCAo) using [^{99m}Tc]hexamethylpropyleneamine oxime ([^{99m}Tc]HMPAO). [^{99m}Tc]HMPAO μSPECT was acquired in $n = 14$ animals 24 hours after tMCAo. T2-weighted (T2w) micro magnetic resonance imaging (μMRI) was conducted 14 days after tMCAo in the same animals to determine the infarct volume. (**A**) Representative images of two examples with different degrees of perfusion deficit and their corresponding T2w-μMR images 14 days after tMCAo. Color scales were adjusted and normalized to the injected activity (MBq). Data are expressed as standardized uptake values (SUVs). (**B**) Depending on the perfusion deficit after 24 hours, varying degrees of infarct volumes were measured. The percentage of remaining ipsilateral relative cerebral blood flow (rCBF) (24 hours after tMCAo) was negatively correlated with the ischemic volume (percentage of whole brain) 14 days after tMCAo (Spearman correlation analysis; $R^2 = -0.66$; $P < 0.010$, $n = 14$).

Figure 2. Temporal dynamics of [^{18}F]DPA-714 and [^{18}F]BR-351 uptake after transient middle cerebral artery occlusion (tMCAo). Dual micro positron emission tomography (μPET) imaging employing [^{18}F]DPA-714 and [^{18}F]BR-351 was performed at four different time points after tMCAo (24 to 48 hours, 7 days, 14 days, and 21 days). Lesion to contralateral (L/C) ratios were calculated. (**A**) Representative images of different animals showing time-dependent radiotracer uptake were depicted at areas with the largest/highest extent of radiotracer uptake at a given time point. (**B**) [^{18}F]DPA-714 uptake was significantly increased from day 7 (L/C: 1.77 ± 0.39; ANOVA, $^*P < 0.05$; $n = 8$), peaked at day 14 (L/C: 2.81 ± 0.76; ANOVA, $^{***}P < 0.001$; $n = 8$), and was still significantly elevated 21 days after tMCAo (L/B: 2.14 ± 0.46; ANOVA, $^{***}P < 0.001$; $n = 7$). [^{18}F]BR-351 was significantly increased after 24 to 48 hours after tMCAo (L/B: 1.37 ± 0.19; ANOVA, $^*P < 0.05$; $n = 8$), and 7 days (L/B: 1.47 ± 0.39; ANOVA, $^*P < 0.05$; $n = 8$). (**C**) Individual quantification of [^{18}F]DPA-714 (left) and [^{18}F]BR-351 (right). [^{18}F]DPA-714 uptake is significantly increased in the infarct compared with the contralateral reference region at day 7 (t-test, $^{**}P > 0.01$; $n = 8$), day 14 (t-test, $^{***}P < 0.001$; $n = 8$) and day 21 (t-test, $^{***}P < 0.001$; $n = 7$). [^{18}F]BR-351 uptake is significantly increased in the infarct 24 to 48 hours (t-test, $^*P < 0.05$; $n = 8$) and 7 days (t-test, $^*P < 0.05$; $n = 8$) after tMCAo. Data are represented as ratio $\pm$ s.d.

[18F]DPA-714 and [18F]BR-351 Micro Positron Emission Tomography Reveals Time-Dependent Increased Radiotracer Uptake from Acute (24 to 48 Hours) to Chronic (up to 21 Days) Phases After Transient Middle Cerebral Artery Occlusion

Dual-tracer μPET imaging employing [18F]DPA-714 and [18F]BR-351 was performed at four different time points after tMCAo (24 to 48 hours, 7 days, 14 days, and 21 days). The μPET imaging of microglia and protease activity after tMCAo showed a time-dependent increase in radiotracer uptake. For quantification of imaging data, lesion to contralateral (L/C) ratios were calculated.

In total, $n = 31$ animals underwent successful multitracer imaging followed by T2w-μMRI. The [18F]DPA-714 uptake ratio was significantly higher in the lesioned area compared with the contralateral site starting at day 7 (L/C: 1.77 ± 0.64; $P < 0.001$; $n = 8$)

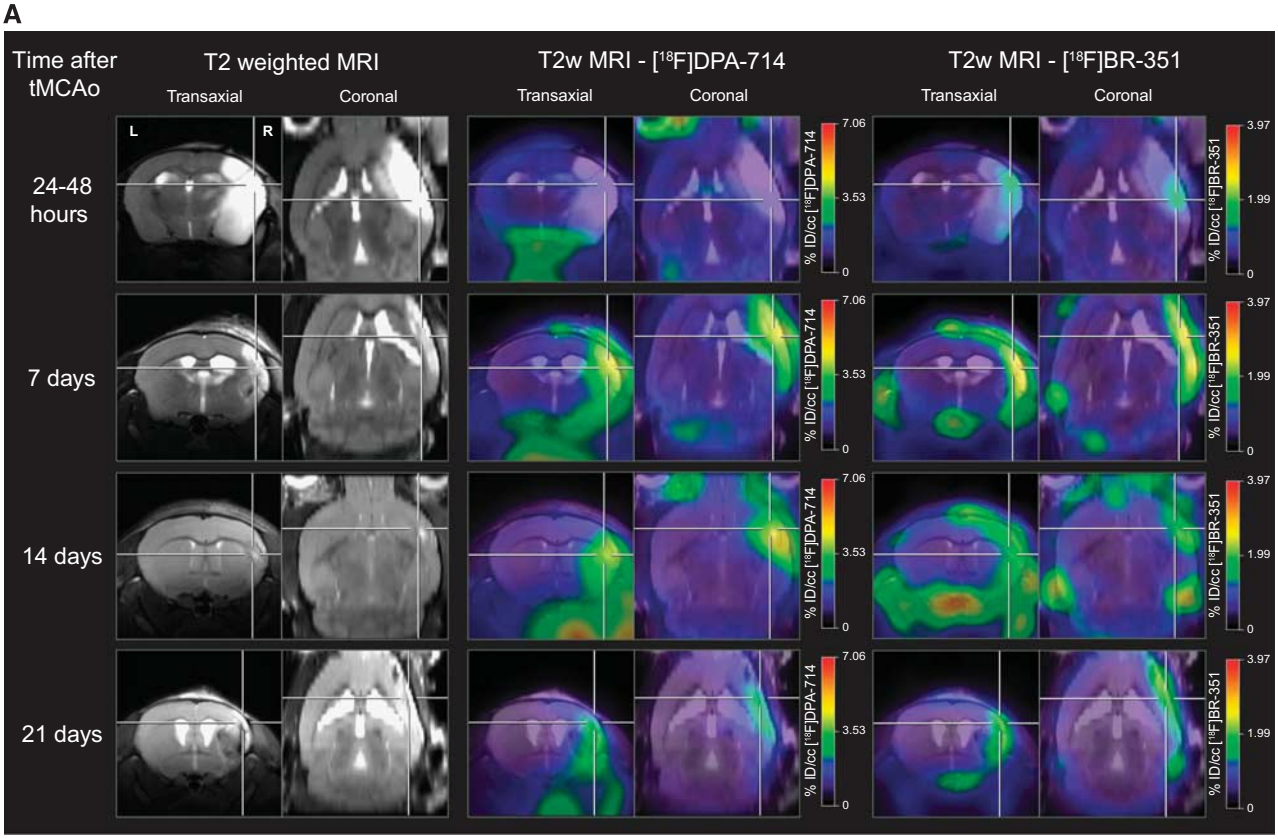

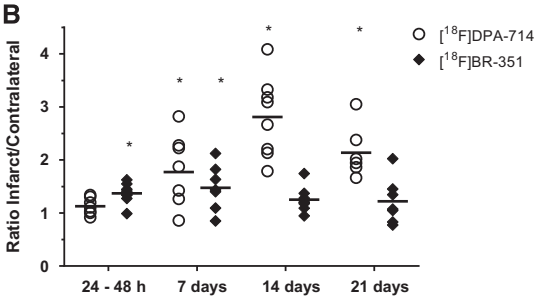

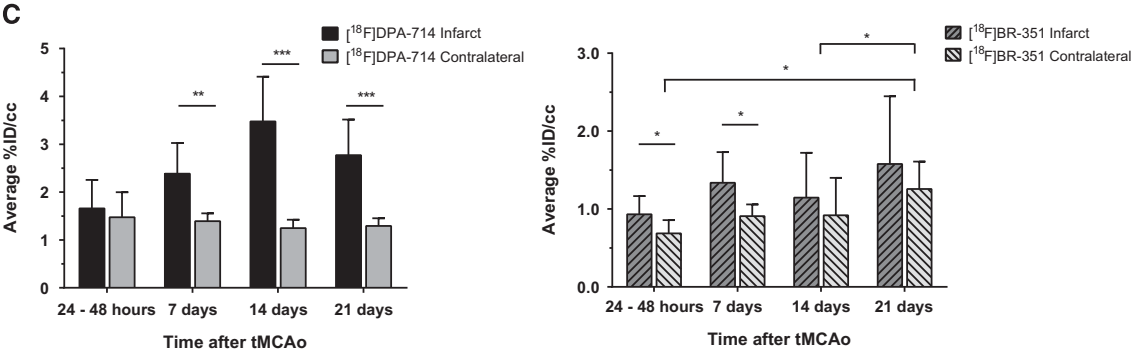

after tMCAo. [^{18}F]DPA-714 peaked after 14 days (L/C: 2.81 ± 0.76; $P < 0.001$; $n = 8$), and was still significantly elevated at day 21 (L/C: 2.14 ± 0.46; $P < 0.001$; $n = 7$) (Figures 2A to 2C). [^{18}F]DPA-714 signal colocalized with the lesion as determined by T2w-μMRI. At 14 days after tMCAo [^{18}F]DPA-714 signal exceeded the lesion (Figure 2A, Supplementary Figure 3).

[^{18}F]BR-351 uptake in the ipsilateral hemisphere was significantly increased at 24 to 48 hours (L/C: 1.37 ± 0.19; $P < 0.05$; $n = 8$) and 7 days (L/C: 1.47 ± 0.39; $P < 0.05$; $n = 8$) after tMCAo (Figures 2A to 2C) but not thereafter. Early (24 to 48 hours after tMCAo) [^{18}F]BR-351 uptake appeared to be restricted to a patch within the lesion, whereas significant tracer uptake at later time points showed a broader extension within the T2w-μMRI determined ischemic lesion. At later time points, [^{18}F]BR-351 tracer uptake was more pronounced in the infarct versus the contralateral regions in some animals, but these differences did not reach statistical significance. The quantitative [^{18}F]DPA-714 and [^{18}F]BR-351 data are summarized in Table 1.

Spatial Validation of [^{18}F]DPA-714 and [^{18}F]BR-351 Micro Positron Emission Tomography with Immunohistochemistry for Translocator Protein and Matrix Metalloproteinase-9

Comparison of μPET imaging data with histology for TSPO and MMP revealed spatial agreement of increased [^{18}F]DPA-714 and [^{18}F]BR-351 uptake with positive TSPO and MMP staining, respectively. In a representative example of a mouse imaged 14 days after tMCAo, the [^{18}F]DPA-714 signal exceeded the lesion indicated by T2w-μMRI (Figures 2 and 3). Overview images of immunohistochemical staining showed spatial agreement of the [^{18}F]DPA-714 signal with TSPO-positive cells, which was confirmed at higher magnification (Figures 3A and 3B). Similar results were obtained for [^{18}F]BR-351, which was spatially related to MMP-9 immunohistochemistry (Figures 3A and 3B).

Cellular Localization of Translocator Protein and Matrix Metalloproteinase-9 Immunoreactivity Validate Micro Positron Emission Tomography Imaging Data

In accordance with the [^{18}F]DPA-714 μPET imaging data, TSPO immunohistochemistry revealed a time-dependent increase in TSPO-positive cells (Figure 4). At 24 to 48 hours after tMCAo, TSPO was found in microglial cells and surrounding larger vessels in the occluded hemisphere. At 7 days, strong TSPO expression was observed in the infarct core and in adjacent areas originating from activated microglia as indicated by Iba-1 staining, and no vessel-associated TSPO staining was detected. At 14 and 21 days after tMCAo, the TSPO staining in the infarct region was more pronounced than at day 7. Double immunofluorescence staining revealed that Iba-1-positive microglia expressed TSPO (Figure 4). No TSPO immunoreactivity could be detected in the contralateral hemisphere, except at 21 days after tMCAo, where faint TSPO-positive endothelial cells could be found. We could not detect any evidence for astrocytes contributing to the TSPO signal using GFAP staining (data not shown).

Immunohistochemistry for MMP-9 confirmed the dynamics of [^{18}F]BR-351 tracer binding (Figure 4). Early after tMCAo (24 to 48 hours), endothelial and microglial cells showed positive staining for MMP-9, whereas at 7, 14, and 21 days after tMCAo the MMP-9 signal was seen in some positive but also in Iba-1-negative cells. Some of these MMP-9 immunoreactive cells were apoptotic cells according to their fragmented nuclei (data not shown). In all animals where μPET was negative for [^{18}F]BR-351 no positive MMP-9 staining could be observed.

[^{18}F]DPA-714 Uptake 14 Days After Transient Middle Cerebral Artery Occlusion, But Not [^{18}F]BR-351, Correlates to the Perfusion Deficit 24 Hours After Transient Middle Cerebral Artery Occlusion

A total of $N = 6$ animals underwent [^{99m}TcHMPAO μSPECT perfusion imaging and received dual μPET imaging for [^{18}F]DPA-714 and [^{18}F]BR-351 at 14 days after tMCAo. In the ischemic region, increased [^{18}F]DPA-714 radiotracer uptake values (%ID) correlated significantly with the blood perfusion deficit as measured by [^{99m}Tc]HMPAO μSPECT ($R^2 = 0.83$; $P < 0.05$; $n = 6$) (Figure 5). No correlation with the remaining rCBF could be observed for [^{18}F]BR-351 ($R^2 = 0.12$; $P > 0.05$; $n = 6$).

Sham Surgery Does Not Affect [^{18}F]DPA-714 and [^{18}F]BR-351 Radio Tracer Uptake and Is Significantly Lower than in the Experimental Group

Animals ($N = 4$) underwent sham surgery 7 days after tMCAo. Dual tracer μPET/CT imaging for [^{18}F]DPA-714 and [^{18}F]BR-351 7 days after sham surgery did not reveal increased radiotracer uptake (Supplementary Figure 4A, D). There was no increased binding of [^{18}F]DPA-714 and [^{18}F]BR-351 in the ipsilateral hemisphere compared with the contralateral side (Supplementary Figure 4B, E). Radiotracer uptake ratios were significantly lower in the sham group for [^{18}F]DPA-714 (I/C: 1.04 ± 0.07; $P < 0.05$; $n = 4$) and [^{18}F]BR-351 (I/C: 0.89 ± 0.12; $P < 0.05$; $n = 4$) (Supplementary Figure 4C, F).

DISCUSSION

This is the first multitracer μPET imaging study investigating the temporal and spatial relationship of two critical inflammatory markers after focal cerebral ischemia *in vivo*. Our results suggest a

Table 1. Summary of radio tracer uptake (%ID) of [^{18}F]DPA-714 and [^{18}F]BR-351 over time after tMCAo

		[^{18}F]DPA-714			*[^{18}F]BR-351*		
		%ID/cc			*%ID/cc*		
	Time after tMCAo	*Infarct*	*Contralateral*	*Ratio infarct/contralateral*	*Infarct*	*Contralateral*	*Ratio Infarct/Contralateral*
Average	24–48 hours	1.75	1.52	1.15	0.93	0.68	1.37
s.d.		0.60	0.52	0.15	0.24	0.17	0.19
Average	7 days	2.38	1.39	1.77	1.33	0.91	1.47
s.d.		0.64	0.17	0.64	0.40	0.15	0.40
Average	14 days	3.48	1.25	2.81	1.14	0.92	1.25
s.d.		0.93	0.17	0.76	0.58	0.48	0.24
Average	21 days	2.77	1.29	2.14	1.57	1.25	1.22
s.d.		0.74	0.16	0.46	0.87	0.36	0.43

Abbreviation: tMCAo, transient middle cerebral artery occlusion.

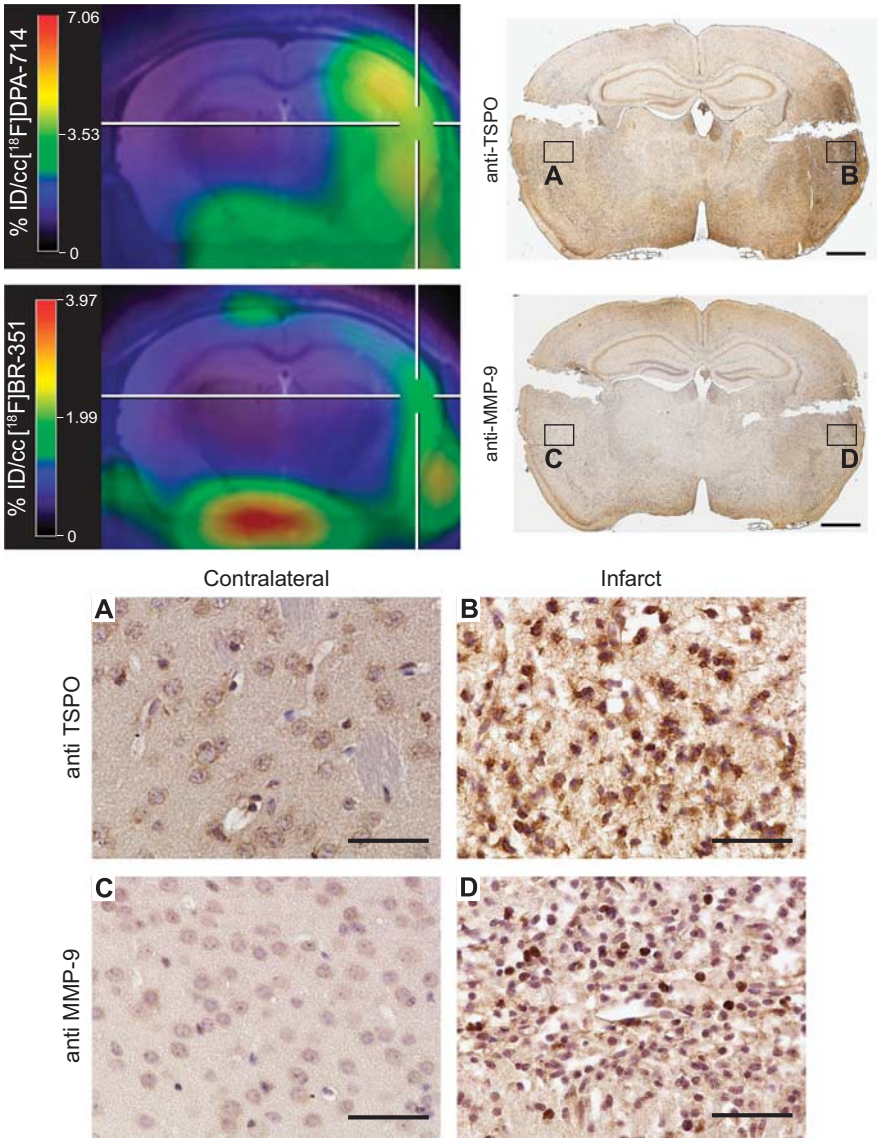

Figure 3. Spatial localization of micro positron emission tomography (μPET)-derived signal validated by immunohistochemistry. In an example of a mouse imaged 14 days after transient middle cerebral artery occlusion (tMCAo) [^{18}F]DPA-714 and [^{18}F]BR-351 signals showed spatial agreement with immunohistochemistry for anti-TSPO and anti-MMP-9 antibody staining, respectively. (**A–D**) Higher magnifications are depicted for control (**A** and **C**) and lesioned (**B** and **D**) areas for anti-TSPO (**A** and **B**) and anti-MMP-9 (**C** and **D**) staining. Scale bar overview scan: 1,000 μm; scale bar (**A**–**D**): 50 μm. MMP-9, matrix metalloproteinase-9; TSPO, translocator protein.

differential time-dependent activation of microglia and MMPs. First, MMPs were found to be upregulated within 1 day after tMCAo with maximal expression at 7 days. At later time points microglial activation started with increased [^{18}F]DPA-714 uptake in the ischemic area reaching a maximum at 14 days. The different time-dependent dynamics and magnitude of the inflammatory parameters suggest that microglial activation and MMP expression after stroke are subsequent or independent phenomena. Immunohistochemical analyses revealed that various cell types (endothelial, microglia, and apoptotic cells) can contribute to MMP activity after ischemic stroke.

After stroke, two molecular markers, TSPO characterizing microglial activation and MMPs are known to be upregulated. To further investigate the link between alterations in cerebral blood flow and activation of microglia and MMPs, it is crucial to employ methods to directly follow these immune responses *in vivo*. As an integrated approach, multitracer ([^{18}F]DPA-714, [^{18}F]BR-351, and [^{99m}Tc]HMPAO) and multimodality (μPET, μSPECT, and μMRI) imaging was applied to obtain anatomic information (μMRI) together with molecular (μPET) and functional (μSPECT) information on various tissue changes after tMCAo in a time-dependent manner. The [^{18}F]DPA-714 TSPO radiotracer showed perfusion deficit-dependent increased uptake with a peak at 14 days after tMCAo as indication of microglial activation. The MMP marker [^{18}F]BR-351 peaked early after stroke and was not related to the severity of the perfusion deficit at 24 hours after tMCAo. Sham surgery did not affect radiotracer uptake 7 days after surgery.

[^{18}F]DPA-714 Micro Positron Emission Tomography Imaging

The cellular and subsequent neuroinflammatory response to ischemic damage is characterized by infiltrating monocytes/macrophages and activation of resident microglia.[17] Activation of microglia involves upregulation of the peripheral benzodiazepine receptor named TSPO.[2,3] Translocator protein is an important mitochondrial target for assessment of neuroinflammation since

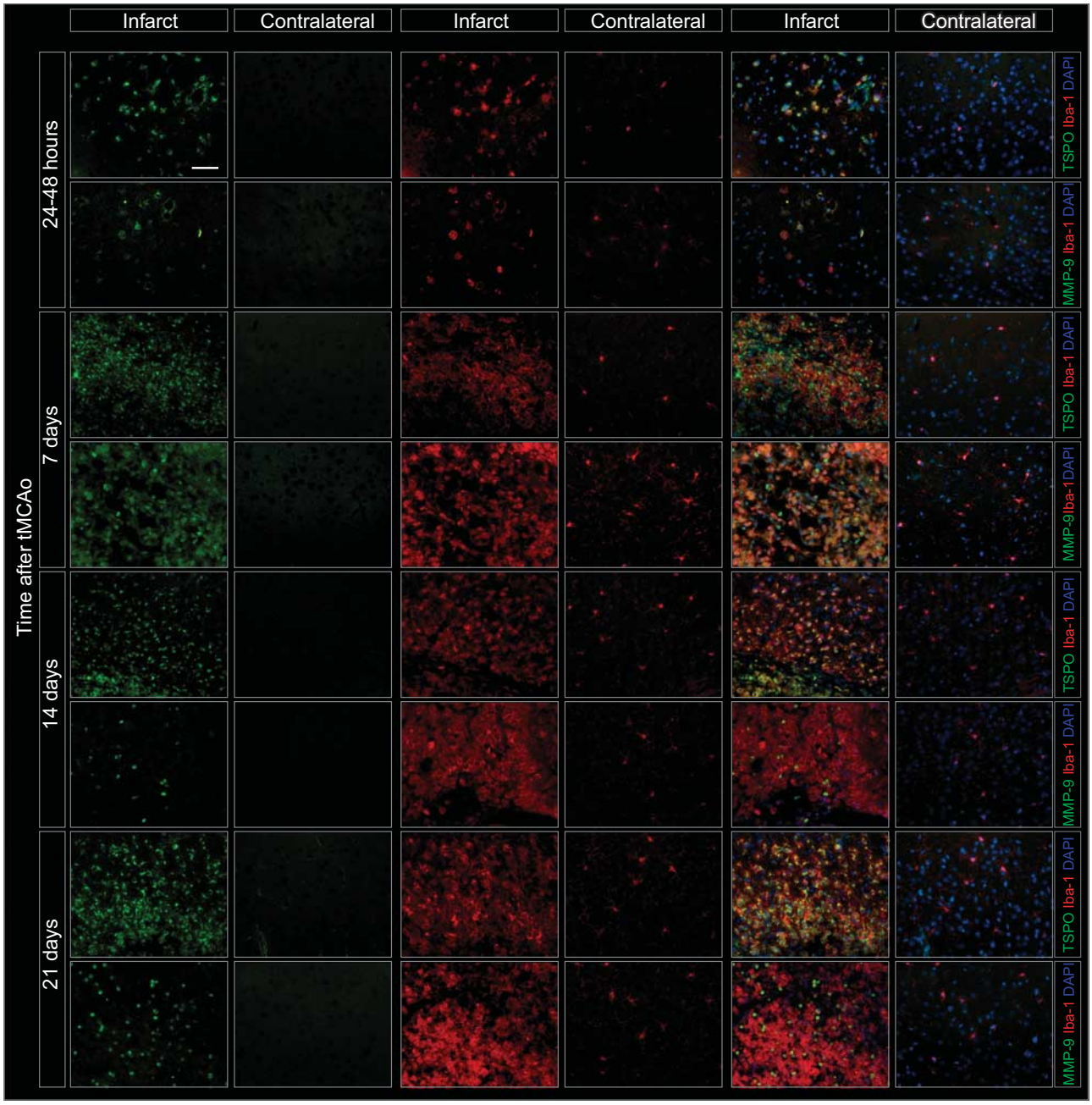

Figure 4. Time course and cellular localization of translocator protein (TSPO) and matrix metalloproteinase 9 (MMP-9) expression after focal cerebral ischemia. Histologic validation of micro positron emission tomography (μPET) data of the same animal as depicted in Figure 2. Images were taken from infarcted areas indicated by the white cross in Figure 2. MMP-9 immunohistochemistry was taken from the infarct core, and TSPO immunohistochemistry from a core-to-periinfarct region, since the massive expression of TSPO in the infarct core did not allow to distinguish single cells. TSPO expression within the infarct is time dependent: 24 to 48 hours after transient middle cerebral artery occlusion (tMCAo) the density of TSPO expressing cells is relatively low, compared with later time points. TSPO was also localized surrounding some larger vessels in the ipsilateral hemisphere at this time. At 7 and 14 days, TSPO staining increased in density with colocalization with microglia cells as defined by Iba-1 staining and morphology. The TSPO signal correlated to the imaging data derived from [^{18}F]DPA-714 μPET. No TSPO immunoreactivity was detected in the contralateral hemisphere, except at 21 days after tMCAo, where faintly TSPO-positive endothelial cells could be found. In correlation with the [^{18}F]BR-351 μPET data, MMP-9 staining was found in the infarct area at 24 to 48 hours after tMCAo in association with the vasculature and microglia (Iba-1), and after 7 days in activated microglia and apoptotic cells. At later time points (14 and 21 days after tMCAo), MMP-9 was mainly found in apoptotic cells. All images were taken with the same magnification. Scale bar: 100 μm.

under physiologic conditions basal expression levels are low (microglia, astrocytes, endothelial and smooth muscle cells, subpial glia, intravascular monocytes, and ependymal cells). In contrast, it is highly upregulated after a neuroinflammatory stimulus in glial cells (microglia, astrocytes) and macrophages.[1,3,18,19]

In the past 30 years, various TSPO ligands have been designed to study microglia-based neuroinflammation *in vivo*.[1] One of the most important TSPO radiotracers used is [^{11}C]PK11195.[1] This tracer shows relatively low signal-to-background ratios, high unspecific binding, but is hampered by a short half-life. Therefore,

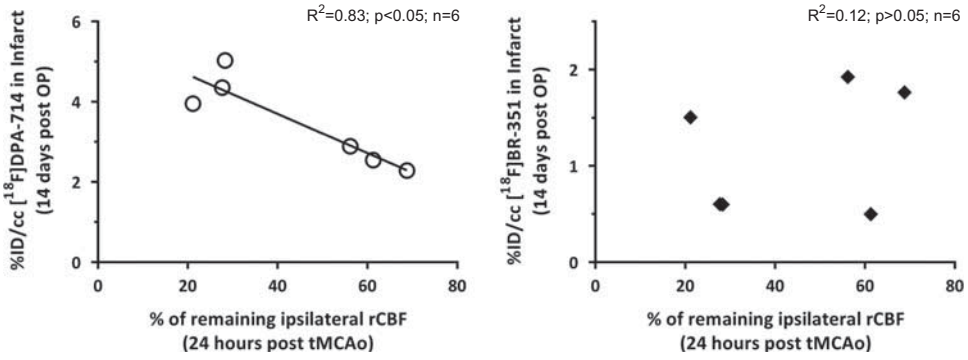

Figure 5. [^{18}F]DPA-714, but not [^{18}F]BR-351, uptake after 14 days correlates inversely with relative cerebral blood flow (rCBF) 24 hours after transient middle cerebral artery occlusion (tMCAo). [^{18}F]DPA-714 and [^{18}F]BR-351 uptake were correlated to the perfusion deficits as measured by [^{99m}Tc]hexamethylpropyleneamine oxime ([^{99m}Tc]HMPAO) micro single photon emission computed tomography (μSPECT). [^{18}F] DPA-714 uptake in the infarct inversely correlated to the percentage of remaining ipsilateral rCBF 24 hours after tMCAo (Spearman correlation analysis; $R^2 = 0.83$; $^*P < 0.05$, $n = 6$). This phenomenon was not observed for [^{18}F]BR-351.

various improved radioligands for TSPO have been developed (reviewed by Jacobs *et al*[1]) including [^{18}F]DPA-714. Compared with [^{11}C]PK11195, [^{18}F]DPA-714 has a relatively low brain uptake under standard physiologic conditions and improved bioavailability, higher specificity, and favorable signal-to-noise ratios in selected disease models.[18,20] This, together with the advantage of a longer half-life of the positron emitter fluorine-18 radio isotope, makes [^{18}F]DPA-714 highly attractive for *in vivo* imaging of microglia activation in animal models as well as for future clinical application. Up to now [^{18}F]DPA-714 has been investigated in several pathologic conditions such as glioblastoma, experimental auto immune encephalomyelitis, experimental neuroinflammation, herpes encephalitis, abdominal aneurysms, and experimental stroke in rats (reviewed by Jacobs *et al*[1]). In particular, in a rat model of cerebral ischemia, a comparative study between [^{11}C] PK11195 and [^{18}F]DPA-714 revealed the superiority of [^{18}F]DPA-714 in terms of an improved signal-to-noise ratio for [^{18}F]DPA-714.[20]

In the current investigation, [^{18}F]DPA-714 μPET imaging revealed a time-dependent increase in uptake in the infarcted region starting from day 7 up to day 21 after tMCAo with a peak at 14 days. This is in agreement with the findings of Martín *et al*[21] that showed increased [^{18}F]DPA-714 binding in the ipsilateral hemisphere at day 7, peaking at day 11 after tMCAo,[21] and with an autoradiographic *ex vivo* study in mice showing the highest [^{3}H] DPA-714 binding at day 14 after tMCAo.[22] However, in the latter study only days 1, 3, and 14 after tMCAo were analyzed.[22] In contrast to our study, where DPA-714 uptake was related to the severity of postischemic hypoperfusion (Figure 5), Harhausen *et al*[22] did not find a relation between lesion volume and [^{3}H] DPA-714 binding. It should be pointed out that at the histologic level, a substantial number of microglial cells are TSPO positive already at 24 to 48 hours after tMCAo (Figure 4). Obviously, this level of TSPO expression or this density of TSPO-positive microglia cells is below or at the detection limit of DPA-714 μPET.

It has been reported that not only microglia but also astroglia contribute to the TSPO signal,[19,21] although in stroke, microglial cells seem to be the main source of TSPO expression. We did not detect TSPO-positive astrocytes at any of the time points using immunohistochemical analyses.

Also, another study in an Alzheimer's disease mouse model showed that TSPO upregulation in microglial cells was associated with deleterious neuronal damage, whereas TSPO expression in astrocytes was an indicator of neurotrophic support.[23] It should be pointed out that currently all TSPO tracers including [^{18}F]DPA-714 cannot distinguish between the different microglial phenotypes (primed, neurotoxic, neuroprotective, others) *in vivo*. For this purpose, the development of new microglia phenotype-specific probe/target combinations is necessary. Interestingly, we found that microglial activation as measured by [^{18}F]DPA-714 was related to the extent of perfusion deficits as assessed by [^{99m}Tc] HMPAO μSPECT 24 hours after tMCAo suggesting that the severity of ischemia may be the stimulus for microglia activation. It should be pointed out that hemodynamic changes[24] and inflammatory alterations[25] within the contralateral hemisphere may have led to an underestimation of L/B ratios. Furthermore, it has been shown that T2 values can resolve to normal values or increase depending on the type of lesion, i.e., initial cortical or no cortical involvement.[26] This might have led to underestimation of μPET quantification parameters at time point >7 days.

[^{18}F]BR-351 Micro Positron Emission Tomography Imaging

MMPs have been shown to be key players in stroke pathogenesis. They are associated with blood–brain barrier damage, hemorrhagic transformation, and vasogenic edema formation.[7,27,28] Over-simplification of MMPs as purely extracellular matrix degrading enzymes should be avoided since *in vivo* evidence that MMPs degrade extracellular matrix is lacking.[29] MMPs have been shown to be involved in modulating inflammatory and immune responses both positively and negatively by processing signaling molecules and by affecting cellular migration.[8] As an example, IL-1ß and TNF-alpha released by microglia/macrophages are tightly regulated by MMPs.[30]

Several approaches have been undertaken to study MMPs in stroke and other pathologies *in vivo*.[31–36] In the case of cerebral ischemia, studies to date have exclusively used MMP-activatable near-infrared MMPSense fluorescent probes.[36,37] However, near-infrared imaging have low tissue penetration and the inability to correct for scatter and attenuation making it unsuitable for clinical application. Therefore, in our study we used the newly developed radiofluorinated hydroxamate-based MMP inhibitor [^{18}F]BR-351, which is based on CGS27023A 125966 and binds to activated forms of MMP-2 ($IC_{50} = 4$ nmol/L), -8 (2 nmol/L), -9 (50 nmol/L), and -13 (11 nmol/L).[38] [^{18}F]BR-351 uptake was observed to be increased in the infarct VOI as early as 24 to 48 hours after tMCAO reaching a maximum at 7 days. No significant differences between the time points analyzed thereafter could be identified using pairwise comparisons. This is in accordance with the previous findings showing that activated MMP-9 can be detected at 12 to 24 hours after permanent MCAo in mice,[39] rats,[9] and non-human primates.[5] In these studies, MMP-9 activity was reported to peak 24 hours after MCAo with levels persisting for 5 days, and basal levels being reestablished at 15 days. In contrast to MMP-9, zymographic analyses of MMP-2 expression indicated persisting

low level expression up to 30 days after tMCAo.[9] It should be pointed out that various cell types seem to contribute to MMP-9 expression after stroke.[9] The investigation of the cellular source of MMPs was not in the scope of the work, but the analysis of the relation between MMP-9 activity with regards to microglia activity as assessed by Iba-1. Early after tMCAo, MMP-9 has been reported in association with endothelial cells and neutrophils,[9,10] whereas after 7 days microglial cells have been reported to express MMP-9.[9] Other studies suggest that astrocytes and neurons are also MMP-9 positive after 7 and 14 days.[10] Moreover, in our study at 7 days after tMCAo MMP-9 expression was found in cells with fragmented nuclei (Figure 4) suggesting an associated role in apoptotic processes or to cells undergoing secondary necrosis.[40,41] Longitudinal *in vivo* imaging of MMPs, therefore, may allow the investigation of different pathophysiologic processes after tMCAo with early [^{18}F]BR-351 signals resembling activation of MMPs in the vasculature and subsequent blood–brain barrier opening, intermediate time points (7 to 14 days after tMCAo) indicating activation of microglia and apoptosis, and later time points (14 to 21 days after tMCAo) marking MMP-related neoangiogenesis.[10] It has been shown that early inhibition of MMP-9 has a beneficial role,[39] whereas late inhibition has detrimental effects[10] on stroke outcome. This highlights the fact that longitudinal imaging of MMP activity *in vivo* by means of [^{18}F]BR-351 and PET could serve as a potential tool to study MMP-modulatory therapies.

[^{99m}Tc]-Hexamethylpropyleneamine Oxime Micro Single Photon Emission Computed Tomography Imaging

The comparison of rCBF at 24 hours after stroke (as measured by μSPECT) with stroke volumes (as measured by μMRI) at 14 days revealed a negative correlation. This supports the use of [^{99m}Tc]HMPAO μSPECT as predictive marker of lesion size/severity 24 hours after tMCAo, as already indicated in clinical trials predicting neurologic outcome using [^{99m}Tc]HMPAO μSPECT.[42] Moreover, [^{99m}Tc]HMPAO as a predictive marker of lesion size allowed us to correlate the lesion size with the extent of microglial activation.

Even though Doppler measurements during the operation suggested successful reopening of the MCA after transient occlusion, [^{99m}Tc]HMPAO images 24 hours after tMCAo suggested variable reductions of rCBF in the ipsilateral hemisphere, which is in accordance with recent data obtained in rats 2 hours after tMCAo.[43] Also, the latter model of perfusion imaging employing [^{13}N]Ammonia showed initial ipsilateral hypoperfusion with rCBF reductions to 40%, followed by normalization and hyperperfusion.[43] Possible explanations for persisting rCBF disturbances after transient MCAo could be that (1) the surgical procedure itself leads to thrombus formation and secondary infarctions due to endothelial damage; (2) upregulation of contractile receptors (e.g., endothelin B) leads to vasoconstriction after tMCAo;[44] and (3) metabolic[45] disturbances and/or oxido-reductive states[46] 24 hours after tMCAo affect the conversion of [^{99m}Tc]HMPAO from a lipophilic to a hydrophilic derivative, independent of blood flow. The postischemic hypoperfusion 24 hours after tMCAo can further be attributed to the 'no-reflow phenomenon'. It has been related to the narrowing of capillaries[47] and loss of both arteriolar dilating mechanisms and cerebrovascular reactivity.[48]

Taken together, the mechanisms of tracer uptake of [^{99m}Tc]HMPAO may not exclusively be perfusion dependent. Pathologic conditions like cerebral ischemia lead to complex molecular, cellular, and physiologic alterations, which could influence tracer uptake and which have to be considered in the interpretation of [^{99m}Tc]HMPAO-based data. Nevertheless, our data imply that [^{99m}Tc]HMPAO is a valuable early predictive marker of stroke outcome.

CONCLUSIONS

Our results show that dynamic inflammatory responses involving activation of microglia and MMPs after stroke can be non-invasively localized and quantified by dual-tracer μPET imaging employing [^{18}F]DPA-714 and [^{18}F]BR-351. For interpretation, additional μCT, μMRI, and μSPECT imaging parameters were used. To our knowledge, this is the first multimodal imaging study employing various radiotracers and imaging technologies to reveal insight into the complex spatial and temporal pathophysiologic, cellular, and molecular consequences after stroke *in vivo*. First in men studies are currently performed with [^{18}F]DPA-714 and [^{18}F]BR-351 in several neurologic and cardiovascular pathologies.

The combination of MMP and microglia imaging may allow the establishment and evaluation of novel treatment paradigms targeting the postischemic phase to modulate detrimental and beneficial MMP and microglial functions to minimize secondary brain damage and promote regeneration after stroke. For this purpose, dedicated probe/target combinations have to be developed to enable the noninvasive differentiation between various microglial phenotypes and MMPs associated with different functions (beneficial versus deleterious) after stroke.

AUTHOR CONTRIBUTIONS

BZ conducted the experiments, designed the figures, and drafted the manuscript. TV conducted the experiments and drafted the manuscript. LW and CF designed and performed the μMRI studies, AV performed the μSPECT studies and analysis, SW, AF, and KK synthesized [^{18}F]DPA-714, [^{18}F]BR-351, and [^{99m}Tc]HMPAO. SH supported the μPET and μSPECT imaging. FD helped in setting up the [^{18}F]DPA-714 synthesis in Münster. SP was involved in data analysis and discussion. AP helped in establishing the tMCAo model in Münster and helped in data analysis and interpretation. BT helped in setting up the [^{18}F]DPA-714 synthesis in Münster and was involved in data interpretation. MS helped in application of [^{18}F]BR-351 data analysis and interpretation. LS helped in histologic interpretation of MMP activity. MK performed and advised on tMCAo surgeries and histology. AHJ designed the study, was involved in data analysis and interpretation, drafted the manuscript.

DISCLOSURE/CONFLICT OF INTEREST

The authors declare no conflict of interest.

ACKNOWLEDGMENTS

The authors thank M Kattenbeck, S Köster, C Bätza, R Priebe, S Bouma, F Breuer, I Hoppe, C Möllmann, and D Reinhardt for their excellent technical support.

REFERENCES

1 Jacobs AH, Tavitian B. consortium Inm. Noninvasive molecular imaging of neuroinflammation. *J Cereb Blood Flow Metab* 2012; **32**: 1393–1415.
2 Papadopoulos V, Baraldi M, Guilarte TR, Knudsen TB, Lacapère JJ, Lindemann P *et al.* Translocator protein (18kDa): new nomenclature for the peripheral-type benzodiazepine receptor based on its structure and molecular function. *Trends Pharmacol Sci* 2006; **27**: 402–409.
3 Chen MK, Guilarte TR. Translocator protein 18 kDa (TSPO): molecular sensor of brain injury and repair. *Pharmacol Ther* 2008; **118**: 1–17.
4 Del Zoppo GJ. Inflammation and the neurovascular unit in the setting of focal cerebral ischemia. *Neuroscience* 2009; **158**: 972–982.
5 Heo JH, Lucero J, Abumiya T, Koziol JA, Copeland BR, del Zoppo GJ. Matrix metalloproteinases increase very early during experimental focal cerebral ischemia. *J Cereb Blood Flow Metab* 1999; **19**: 624–633.
6 Del Zoppo GJ. The neurovascular unit, matrix proteases, and innate inflammation. *Ann NY Acad Sci* 2010; **1207**: 46–49.
7 Del Zoppo GJ, Frankowski H, Gu YH, Osada T, Kanazawa M, Milner R *et al.* Microglial cell activation is a source of metalloproteinase generation during hemorrhagic transformation. *J Cereb Blood Flow Metab* 2012; **32**: 919–932.
8 McQuibban GA, Gong JH, Wong JP, Wallace JL, Clark-Lewis I, Overall CM. Matrix metalloproteinase processing of monocyte chemoattractant proteins generates

CC chemokine receptor antagonists with anti-inflammatory properties in vivo. *Blood* 2002; **100**: 1160–1167.
9 Romanic AM, White RF, Arleth AJ, Ohlstein EH, Barone FC. Matrix metalloproteinase expression increases after cerebral focal ischemia in rats: inhibition of matrix metalloproteinase-9 reduces infarct size. *Stroke* 1998; **29**: 1020–1030.
10 Zhao BQ, Wang S, Kim HY, Storrie H, Rosen BR, Mooney DJ *et al.* Role of matrix metalloproteinases in delayed cortical responses after stroke. *Nat Med* 2006; **12**: 441–445.
11 Wagner S, Faust A, Breyholz HJ, Schober O, Schafers M, Kopka K. The MMP inhibitor (R)-2-(N-benzyl-4-(2-[18F]fluoroethoxy)phenylsulphonamido)-N-hydroxy-3-methylbuta namide: Improved precursor synthesis and fully automated radiosynthesis. *Appl Radiat Isot* 2011; **69**: 862–868.
12 Engel O, Kolodziej S, Dirnagl U, Prinz V. Modeling stroke in mice - middle cerebral artery occlusion with the filament model. *J Vis Exp* 2011; **47**: 2423.
13 James ML, Fulton RR, Vercoullie J, Henderson DJ, Garreau L, Chalon S *et al.* DPA-714, a new translocator protein-specific ligand: synthesis, radiofluorination, and pharmacologic characterization. *J Nucl Med* 2008; **49**: 814–822.
14 Vrachimis A, Hermann S, Mathe D, Schober O, Schafers M. Systematic evaluation of 99mTc-tetrofosmin versus 99mTc-sestamibi to study murine myocardial perfusion in small animal SPECT/CT. *EJNMMI Res* 2012; **2**: 21.
15 Schäfers KP, Reader AJ, Kriens M, Knoess C, Schober O, Schäfers M. Performance evaluation of the 32-module quadHIDAC small-animal PET scanner. *J Nucl Med* 2005; **46**: 996–1004.
16 Vollmar SCJ, Sue M, Klein J, Jacobs AH, Herholz K. *VINCI-Volume Imaging in Neurological Research, Co-Registration and ROIs Forschung und wissenschaftliches Rechnen 2003*. Göttingen: Gesellschaft für Wissenschaftliche Datenverarbeitung, 2004; 115–131.
17 Ceulemans AG, Zgavc T, Kooijman R, Hachimi-Idrissi S, Sarre S, Michotte Y. The dual role of the neuroinflammatory response after ischemic stroke: modulatory effects of hypothermia. *J Neuroinflammation* 2010; **7**: 74.
18 Chauveau F, Van Camp N, Dollé F, Kuhnast B, Hinnen F, Damont A *et al.* Comparative evaluation of the translocator protein radioligands 11C-DPA-713, 18F-DPA-714, and 11C-PK11195 in a rat model of acute neuroinflammation. *J Nucl Med* 2009; **50**: 468–476.
19 Lavisse S, Guillermier M, Herard AS, Petit F, Delahaye M, Van Camp N *et al.* Reactive astrocytes overexpress TSPO and are detected by TSPO positron emission tomography imaging. *J Neurosci* 2012; **32**: 10809–10818.
20 Boutin H, Prenant C, Maroy R, Galea J, Greenhalgh AD, Smigova A *et al.* [18F] DPA-714: direct comparison with [11C]PK11195 in a model of cerebral ischemia in rats. *PLoS One* 2013; **8**: e56441.
21 Martín A, Boisgard R, Thézé B, Van Camp N, Kuhnast B, Damont A *et al.* Evaluation of the PBR/TSPO radioligand [(18)F]DPA-714 in a rat model of focal cerebral ischemia. *J Cereb Blood Flow Metab* 2010; **30**: 230–241.
22 Harhausen D, Sudmann V, Khojasteh U, Muller J, Zille M, Graham K *et al.* Specific Imaging of Inflammation with the 18kDa Translocator Protein Ligand DPA-714 in Animal Models of Epilepsy and Stroke. *PLoS One* 2013; **8**: e69529.
23 Ji B, Maeda J, Sawada M, Ono M, Okauchi T, Inaji M *et al.* Imaging of peripheral benzodiazepine receptor expression as biomarkers of detrimental versus beneficial glial responses in mouse models of Alzheimer's and other CNS pathologies. *J Neurosci* 2008; **28**: 12255–12267.
24 Martín A, Macé E, Boisgard R, Montaldo G, Thézé B, Tanter M *et al.* Imaging of perfusion, angiogenesis, and tissue elasticity after stroke. *J Cereb Blood Flow Metab* 2012; **32**: 1496–1507.
25 Burrows FE, Bray N, Denes A, Allan SM, Schiessl I. Delayed reperfusion deficits after experimental stroke account for increased pathophysiology. *J Cereb Blood Flow Metab* 2014; **35**: 277–284.
26 Wegener S, Weber R, Ramos-Cabrer P, Uhlenkueken U, Sprenger C, Wiedermann D *et al.* Temporal profile of T2-weighted MRI distinguishes between pannecrosis and selective neuronal death after transient focal cerebral ischemia in the rat. *J Cereb Blood Flow Metab* 2006; **26**: 38–47.
27 Montaner J, Alvarez-Sabin J, Molina CA, Angles A, Abilleira S, Arenillas J *et al.* Matrix metalloproteinase expression is related to hemorrhagic transformation after cardioembolic stroke. *Stroke* 2001; **32**: 2762–2767.
28 Del Zoppo GJ, Milner R, Mabuchi T, Hung S, Wang X, Berg GI *et al.* Microglial activation and matrix protease generation during focal cerebral ischemia. *Stroke* 2007; **38**: 646–651.
29 Sorokin L. The impact of the extracellular matrix on inflammation. *Nat Rev Immunol* 2010; **10**: 712–723.
30 Rodriguez D, Morrison CJ, Overall CM. Matrix metalloproteinases: what do they not do? New substrates and biological roles identified by murine models and proteomics. *Biochim Biophys Acta* 2010; **1803**: 39–54.
31 Weissleder R, Tung CH, Mahmood U, Bogdanov A, Jr. In vivo imaging of tumors with protease-activated near-infrared fluorescent probes. *Nat Biotechnol* 1999; **17**: 375–378.
32 Schafers M, Riemann B, Kopka K, Breyholz HJ, Wagner S, Schafers KP *et al.* Scintigraphic imaging of matrix metalloproteinase activity in the arterial wall in vivo. *Circulation* 2004; **109**: 2554–2559.
33 Su H, Spinale FG, Dobrucki LW, Song J, Hua J, Sweterlitsch S *et al.* Noninvasive targeted imaging of matrix metalloproteinase activation in a murine model of postinfarction remodeling. *Circulation* 2005; **112**: 3157–3167.
34 Hartung D, Schafers M, Fujimoto S, Levkau B, Narula N, Kopka K *et al.* Targeting of matrix metalloproteinase activation for noninvasive detection of vulnerable atherosclerotic lesions. *Eur J Nucl Med Mol Imaging* 2007; **34**: S1–S8.
35 Lancelot E, Amirbekian V, Brigger I, Raynaud JS, Ballet S, David C *et al.* Evaluation of matrix metalloproteinases in atherosclerosis using a novel noninvasive imaging approach. *Arter Thromb Vasc Biol* 2008; **28**: 425–432.
36 Klohs J, Baeva N, Steinbrink J, Bourayou R, Boettcher C, Royl G *et al.* In vivo near-infrared fluorescence imaging of matrix metalloproteinase activity after cerebral ischemia. *J Cereb Blood Flow Metab* 2009; **29**: 1284–1292.
37 Barber PA, Rushforth D, Agrawal S, Tuor UI. Infrared optical imaging of matrix metalloproteinases (MMPs) up regulation following ischemia reperfusion is ameliorated by hypothermia. *BMC Neurosci* 2012; **13**: 76.
38 Wagner S, Breyholz HJ, Höltke C, Faust A, Schober O, Schäfers M *et al.* A new 18F-labelled derivative of the MMP inhibitor CGS 27023A for PET: radiosynthesis and initial small-animal PET studies. *Appl Radiat Isot* 2009; **67**: 606–610.
39 Asahi M, Asahi K, Jung JC, del Zoppo GJ, Fini ME, Lo EH. Role for matrix metalloproteinase 9 after focal cerebral ischemia: effects of gene knockout and enzyme inhibition with BB-94. *J Cereb Blood Flow Metab* 2000; **20**: 1681–1689.
40 Yang Y, Candelario-Jalil E, Thompson JF, Cuadrado E, Estrada EY, Rosell A *et al.* Increased intranuclear matrix metalloproteinase activity in neurons interferes with oxidative DNA repair in focal cerebral ischemia. *J Neurochem* 2010; **112**: 134–149.
41 Pirici D, Pirici I, Mogoanta L, Margaritescu O, Tudorica V, Margaritescu C *et al.* Matrix metalloproteinase-9 expression in the nuclear compartment of neurons and glial cells in aging and stroke. *Neuropathology* 2012; **32**: 492–504.
42 Alexandrov A V, Black SE, Ehrlich LE, Bladin CF, Smurawska LT, Pirisi A *et al.* Simple visual analysis of brain perfusion on HMPAO SPECT predicts early outcome in acute stroke. *Stroke* 1996; **27**: 1537–1542.
43 Martin A, Mace E, Boisgard R, Montaldo G, Theze B, Tanter M *et al.* Imaging of perfusion, angiogenesis, and tissue elasticity after stroke. *J Cereb Blood Flow Metab* 2012; **32**: 1496–1507.
44 Povlsen GK, Waldsee R, Ahnstedt H, Kristiansen KA, Johansen FF, Edvinsson L. In vivo experimental stroke and in vitro organ culture induce similar changes in vasoconstrictor receptors and intracellular calcium handling in rat cerebral arteries. *Exp Brain Res* 2012; **219**: 507–520.
45 Colamussi P, Calo G, Sbrenna S, Uccelli L, Bianchi C, Cittanti C *et al.* New insights on flow-independent mechanisms of 99mTc-HMPAO retention in nervous tissue: in vitro study. *J Nucl Med* 1999; **40**: 1556–1562.
46 Blankenberg FG, Kinsman SL, Cohen BH, Goris ML, Spicer KM, Perlman SL *et al.* Brain uptake of Tc99m-HMPAO correlates with clinical response to the novel redox modulating agent EPI-743 in patients with mitochondrial disease. *Mol Genet Metab* 2012; **107**: 690–699.
47 Hauck EF, Apostel S, Hoffmann JF, Heimann A, Kempski O. Capillary flow and diameter changes during reperfusion after global cerebral ischemia studied by intravital video microscopy. *J Cereb Blood Flow Metab* 2004; **24**: 383–391.
48 Leffler CW, Beasley DG, Busija DW. Cerebral ischemia alters cerebral microvascular reactivity in newborn pigs. *Am J Physiol Hear Circ Physiol* 1989; **257**: H266–H271.

Supplementary Information accompanies the paper on the Journal of Cerebral Blood Flow & Metabolism website (http://www.nature.com/jcbfm)